

MODELING OF ANECHOIC CHAMBER USING A BEAM-TRACING TECHNIQUE

B. K. Chung, C. H. Teh, and H. T. Chuah

Faculty of Engineering
Multimedia University
63100 Cyberjaya, Malaysia

Abstract—Building an anechoic chamber involves a substantial investment both financially and in physical space. Hence, there is much interest in trying to reduce the required investment while still maintaining adequate performance. The performance of an anechoic chamber depends on the type, size, and array configuration of the absorber elements as well as the geometry of the screened room on which the inner surfaces are covered with RF absorbers. If the room geometry is designed such that an electromagnetic ray from the transmitter will only reach the receiver antenna after a few reflections, the wave energy may be sufficiently damped after a few bounces off the absorbing walls and ceiling. Hence, lower cost RF absorbers can be used to make the anechoic chamber design more economical. In this paper, a variant of beam-tracing technique is used for modeling of anechoic chamber to study the normalized site attenuation (NSA) performance of the anechoic chamber. This allows the chamber performance to be predicted prior to the actual construction. The major advantage of beam-tracing over ray tracing is the path loss information at multiple receiver locations can be determined simultaneously as opposed to running a ray tracing simulation for each receiver location one at a time. As a result, the computing time is greatly reduced. This feature is particularly useful in calculating the field strength at different heights of the receiving antenna in EMC site calibration procedure. The efficient modeling tool has given rise to the successful design and construction of an asymmetrical shape anechoic chamber that supports various measurement needs including EMC tests at the Multimedia University, Malaysia.

1 Introduction

2 Modeling of EMC Test Chamber

3 Modeling and Measurement Results

4 Conclusion

Acknowledgment

References

1. INTRODUCTION

Electrical and electronic devices must be tested for electromagnetic compatibility (EMC) according to the relevant standards. Manufacturers are required to ensure the levels of EMI emissions from the products comply with the regulatory limits. Open Area Test Site (OATS) which is built on a flat terrain free of reflective obstacles is specified in all the standards for conducting the radiated emission test. The problem with OATS is the exposure to the local electromagnetic ambient environment as well as the weather. As an alternative, a screened room with the walls and ceiling covered with suitable RF absorbers can be used for radiated emission measurement. Leaving the conductive floor not covered with RF absorbers, the facility is known as a semi-anechoic chamber (SAC) and it simulates an OATS.

Large semi-anechoic chambers (SAC) with a measurement distance between the source and the receiving antenna of 10 m are by far the best test environments for EMC tests. The required characteristics of the SAC are defined in ANSI C63.4 and EN50147-2. Most of the European product standards require the emission measurement to be performed at 10-m range. The FCC also requires emission measurement to be performed at 10-m range for Class-A devices, while the use of 3-m range is acceptable for Class-B devices. Large measurement uncertainty is inherent in the measurement at 3-m range [1]. In addition to mutual coupling between the source and the receiver, the antenna factors supplied by the antenna manufacturer may be affected by up to 5 dB in the low frequency range due to interactions with the nearby walls [2]. Despite the problems, the high cost of 10-m range forces most manufacturers of electronic products to invest in 3-m range SAC for pre-compliance tests. Full compliance 10-m range SAC's are only available at a few test laboratories.

A large part of the investment in constructing a SAC is due to the RF absorbers. Pyramidal-shaped absorber requires the height of the pyramid to be greater than quarter wavelength in order to

function efficiently. At 30 MHz, the taper length must be greater than 2.5 m. Thin urethane foam pyramids that are optimized to operate from 200 to 1000 MHz have been combined with ferrite tiles to form a hybrid absorber to cover the required frequency range of 30–1000 MHz [3]. The hybrid absorbers are extremely expensive. In addition, the strength of the room must be strong enough to support the weight of the hybrid absorbers. The special room structure adds to the cost of constructing the anechoic chamber. On the other hand, the use of 2.5-m thick pyramid absorbers requires a screened room size larger than 20 m×10 m×9 m height in order to construct a 10-m range semi-anechoic chamber for EMC tests. The required cost and space are substantial. Hence, there is much interest in trying to reduce the required investment while still maintaining adequate performance.

A microwave anechoic chamber has been constructed at the Multimedia University. The primary objective of the anechoic chamber is to facilitate the research and development in the areas of Antenna and Remote Sensing for frequency range of 3 to 18 GHz. In addition, EMC is also an area of interest of the research group. Hence, the anechoic chamber has been designed to also support EMC tests (30–1000 MHz) without incurring excessive extra cost.

The performance of an anechoic chamber depends on the type, size, and array configuration of the absorber elements as well as the geometry of the screened room on which the inner surfaces are covered with the RF absorbers. If the room geometry is designed such that an electromagnetic ray from the transmitter will only reach the receiver antenna after a few reflections, the wave energy may be sufficiently damped after a few bounces off the absorbing walls and ceiling. Hence, the problem with poorer reflectivity of the RF absorbers at lower frequencies can be overcome and the anechoic chamber design can be more economical. An efficient modeling tool is required so that performance of anechoic chamber with different geometry can be predicted prior to the actual construction.

EMC standards specify that a radiated emission test site shall be validated by means of a set of normalized site attenuation (NSA) measurements. The floor shall be a perfectly conducting ground plane. For a 10-meter range, the horizontal distance between the transmitter antenna and receiver antenna shall be 10 meters. The receiver antenna scans from 1 to 4 meters heights and the maximum signal voltage measured from this scan is recorded. Site attenuation is defined as the ratio of the voltage input to a matched and balanced lossless radiator to that at the output of a similarly matched balanced lossless receiver antenna. NSA is calculated by dividing the site attenuation with the antenna factors of the transmitter and receiver antennas. A

measurement site is considered acceptable for compliance test purposes if the measured NSAs are within ± 4 dB of the theoretical NSA for an ideal site.

In the design of a SAC, the NSA measurement requirements must be considered. A modeling technique to predict the NSA performance prior to the SAC construction must include the effects of placing the transmitter antenna at various locations in the test volume, scanning the receiver antenna from 1–4 m height, reflections from the ground plane, and reflections from the absorber-lined walls and ceiling.

The objective of this paper is to introduce the application of a new beam-tracing technique in the modeling of an EMC test chamber.

2. MODELING OF EMC TEST CHAMBER

The most popular technique for modeling of wave propagation behavior is that of geometrical optics (GO). Rays representations of electromagnetic waves are traced from the transmitter, changing rays direction as they undergo reflection and refraction, and the field quantities of those rays that arrive at the receiver are determined. The Geometrical Theory of Diffraction (GTD) and Uniform Theory of Diffraction (UTD) methods are extension to GO rays to include the effects of diffraction. The behavior of the diffracted wave at edges and corners can be determined from an asymptotic form of the exact solution for simpler canonical problems. For example, the diffraction around a sharp edge is found by considering the asymptotic form of the solution for an infinite wedge. The geometrical optics methods are only accurate when the dimensions of objects being analyzed are large relative to the wavelength of the field.

There are two basic categories of ray tracing propagation models: brute-force shoot and bounce ray (SBR) [4] and image based methods [5]. Conventional SBR methods suffer large kinematics error due to the use of reception sphere. Image based methods do not have such problem. However, without an efficient image generation algorithm, they are not manageable for complex scene, therefore their applications are rather limited. A hybrid SBR-image model [6] that improves the efficiency of image generation has been developed. The choice of SBR technique would govern the performance of the hybrid model. The basic classes of SBR techniques that can be used are ray, tube, and beam approaches.

In the use of ray approach, individual rays are launched and traced. The separation between various rays launched from the transmitter is critical. It must be small enough that two adjacent rays never straddle and miss a potential scatterer or receiver. On

the other hand, it must not be too small that the computation time is excessive due to the huge number of rays. The optimum ray separation is difficult to determine because the ray separation increases with distance. Different ray separation must be used for different scene. Reception has to be validated by a backward tracing process. A significant number of backward tracing efforts may end in invalid reception and discarded. This kind of trivial effort grows with the number of receivers or observation points.

A ray-tube approach where several rays are grouped to form a tube with simple polygon cross section (e.g., triangle or rectangular) has been developed by Chen and Jeng [6]. It enhances the reception validation process by eliminating backward ray tracing of invalid ray paths. A more complicated tube-tracing algorithm is required. Ray separation or tube size remains critical and the concerns of optimum ray separation also apply here.

Improvement using large ray-tubes is provided by a beam-tracing method [7]. Beams with irregular cross section, representing infinite number of rays, are used. Ray separation is not a concern, and the beam size is not critical. Ideally, one beam represents one ray path, in contrast to the large number of rays or ray-tubes required for keeping track of one ray path in the ray or ray-tube approach. The beams also assist in reception test by eliminating trivial backward tracing of invalid ray paths. However, the beam tracing is also the most complicated to code among the SBR techniques.

A variant of beam tracing technique has been developed by Teh and Chuah [8]. Generic polygons are traced instead of the beams. Thus the technique is called polygon tracing method. A generic polygon may consists of one or more polygons which may be concave or convex, self-intersecting or contains holes. Scatterers are modeled as objects with polygonal facets. Reception sphere is not required, giving rise to very low kinematics errors. In a problem where a large number of receivers are involved, a minimum number of beams can cover all the receiver locations. Hence, the required computation time can be dramatically reduced. This feature is particularly useful in calculating the field strength at different heights of the receiving antenna in EMC site calibration procedure.

The polygon tracing method shoots and bounces polygonal projections from the transmitter and its images. The ray-polygon may be transformed to a different polygonal shape when projected onto an arbitrary view plane as illustrated in Figure 1. Each view plane is selected to coincide with a plane object at the scene. The footprint on the view plane represents the region illuminated by the transmitter or the image source.

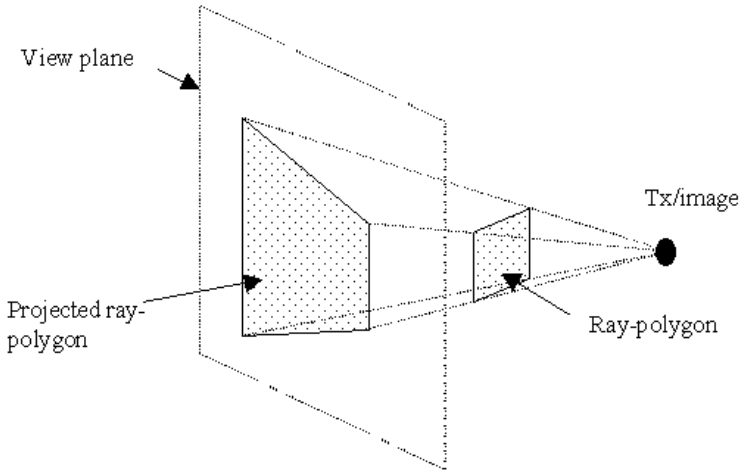


Figure 1. Projection of ray polygon to a view plane.

To cover rays in all directions, the original transmitter ray-polygons may be represented by the 6 faces of a rectangular box enclosing the transmitter. To begin tracing a ray-polygon, the entity (scatterer or receiver) nearest to the source is projected onto the plane containing the ray-polygon. The center of projection (COP) is the position of the source. If the projection of a receiver lies within the ray polygon, it means the receiver will receive a ray from the source. Backward ray tracing is then performed to determine the exact path information for electromagnetic field calculations based on GO and UTD. In the case of a scatterer entity, the overlap area between the projection of the object and the ray-polygon plane indicates the area where the beam energy will be intercepted. Reflection and transmission ray-polygons that take the shape of the illuminated area of the object are created and queued for further tracing to the subsequent scatterer or receiver at the scene. Other area of the object may be illuminated by an adjacent ray-polygon. An illustration of the polygon tracing mechanism is given in Figure 2.

A list of objects at the scene is compiled according to the visibility of the objects from a desired viewpoint in space. The Binary Space Partitioning (BSP) scheme adopted from computer graphics is used for this purpose [9]. It is an extremely efficient method for calculating the visibility relationships among a static group of 3D polygons as seen from an arbitrary viewpoint. When a new viewpoint is specified, the BSP tree can be reused to determine the new visibility order. This

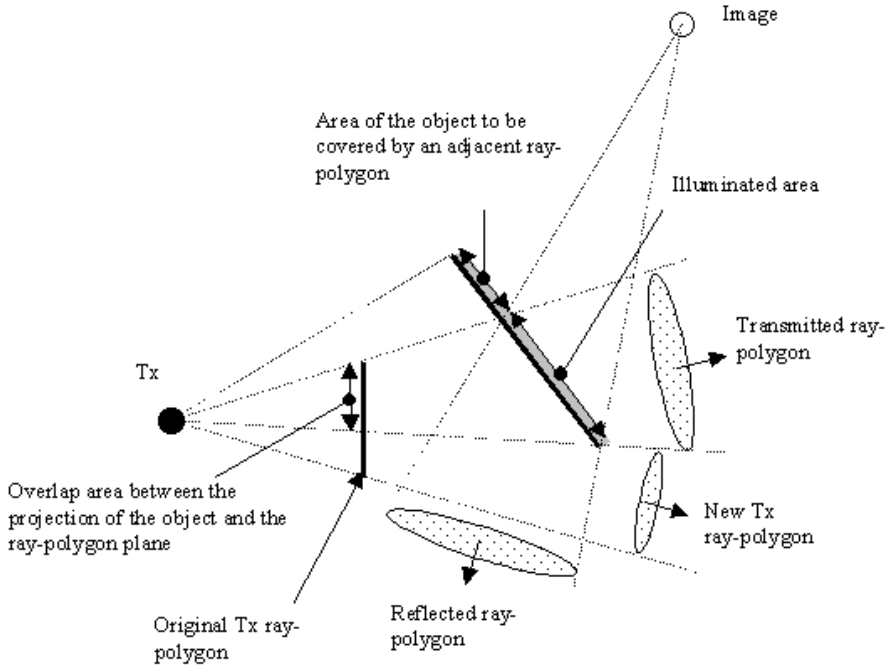
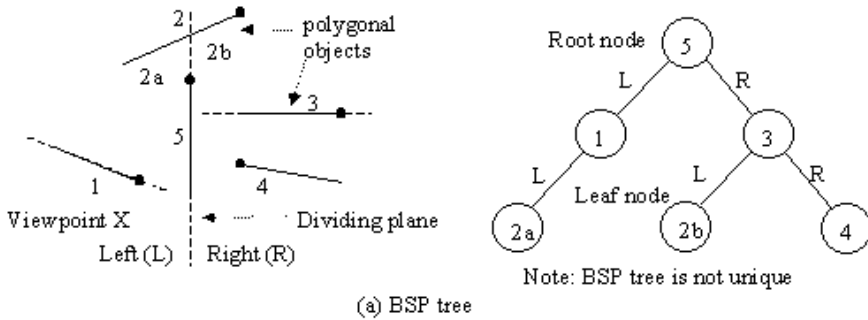


Figure 2. Creation of transmitted and reflected ray-polygons.

feature is very useful in ray-polygon tracing for the various image sources.

In the BSP algorithm, a plane containing one or more of the objects is used to partition the objects at the scene. The objects are then classified according to their relative positions to the dividing plane. Those coincide with the dividing plane form a BSP node while those crossing the plane are split into two, one on the left and one on the right. The partitioning process is repeated recursively on the left set of objects and the right set of objects, generating a binary object tree known as BSP tree (as shown in Figure 3(a)). The relative positions of viewpoint in BSP tree imply the visibility order of objects from the viewpoint (as shown in Figure 3(b)). For example, referring to Figure 3, objects 1 and 2a are at the same side as the viewpoint X relative to object 5. Therefore, they are in front of object 5 as far as viewpoint X is concerned. Objects 2b, 3 and 4 are behind object 5.

From the list of objects ordered according to the visibility from the transmitter, the polygon tracing process starts from the node nearest to the transmitter. Receivers on the same side as the transmitter



Observation	Implication
1. Viewpoint X is on the left of root node (object 5).	Object 2b, 3 & 4 are behind object 5. Object 1 & 2a are in front of object 5.
2. X is on the right of object 1.	Object 2a is behind object 1.
3. X is on the right of object 3.	Object 2b is behind object 3. Object 4 is in front of object 3.
Conclusion	Visibility order is 1-2a-5-4-3-2b

(b) Use of BSP tree to determine visibility order from a viewpoint

Figure 3. Binary space partitioning technique.

relative to the node’s dividing plane have a line of sight (LOS) path. Conversely, receivers on the other side may be obstructed by the node’s objects and their reception test will be conducted after the object projections are clipped from the ray-polygons. For each intersection of object projections and ray-polygons, a reflection and transmission images with the respective ray-polygons are created (as shown in Figure 2). Polygon clipping and intersection are obtained using a readily available generic polygon clipping library [10] based on a modified Vatti algorithm. The ray-polygons then traverse the BSP tree following the visibility order, until they are completely obstructed or the entire BSP tree is traversed. At each BSP node, polygon clipping and intersection, image generation, and reception test are carried out. Figure 4 illustrates an example trace route for a transmitter’s ray-polygon.

To include diffraction, edges of the polygonal object plane that fall within the projection of the ray-polygon are considered. Diffraction ray-polygons are created and traced for their subsequent reflection and transmission. However, projection of the ray-polygon based on

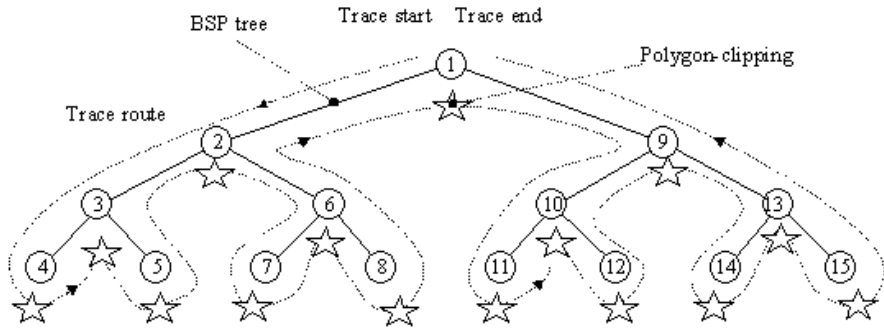


Figure 4. A trace-route example for transmitter's ray-polygon.

the diffraction law is rather complicated. The projection for a straight line may become a curved-line. Since the diffracted wave amplitude is usually very weak, the subsequent reflection, transmission and diffraction may be negligible.

In the modeling of SAC, waves that make more than one bounce off the absorbing walls and ceiling may be assumed negligible if good quality absorbers such as 2.5-m length pyramid or hybrid absorbers are used. A chamber of rectangular shape may be adequate and a simpler ray-tracing method may be developed for modeling of the SAC [11]. However, when shorter pyramidal foam absorber (with poorer reflectivity at frequencies below 1000 MHz) is used, the chamber shape must be optimized in order to meet the site validation requirements for EMC test. Reflected waves after 2 or 3 bounces off the absorbing walls and ceiling may still have significant effect on the NSA results. With optimum chamber geometry designed such that an electromagnetic ray from the transmitter will only reach the receiver antenna after 3 or more reflections, the wave energy may be sufficiently damped (due to absorber return loss and wave propagation loss). The effect on NSA results may be tolerable within the ± 4 dB limits.

The absorber-lined walls and ceiling can be modeled as plane-boundary lossy dielectric with the appropriate effective dielectric constant and effective conductivity or using other modeling methods [12–14]. The floor is modeled as a perfectly conducting plane. The path information of various rays that arrive at multiple receiver locations after a number of reflections and diffraction is determined for electromagnetic field calculations. The NSA can be determined

from the equation below:

$$NSA = \frac{\lambda \cdot R_o}{\eta} \cdot d_{eff} = \frac{\lambda \cdot R_o}{\eta} \cdot \frac{|E_1|}{|E_{obs}|_{\max}} \quad (1)$$

where $|E_1|$ is the electric field strength at a distance of 1 m from the transmitter antenna, $|E_{obs}|$ the electric field strength observed at a receiver location (due to the vector sum of the direct signal and all the reflected waves), λ the wavelength, η the intrinsic wave impedance (377 ohms), and R_o the reference impedance (50 ohms). The largest magnitude of $|E_{obs}|$ is to be found for receiver antenna height scan from 1 m to 4 m.

The computer program simulates a wave is transmitted from a dipole antenna and it propagates in all directions in the form of ray-polygons. For every bounce off the absorbing wall, the electric field strength is multiplied with the absorber reflection coefficient. The absorber model shall be able to determine the degradation of the absorber reflectivity at oblique incidence for parallel and perpendicular polarization.

3. MODELING AND MEASUREMENT RESULTS

A 24-inch thick pyramid absorber is considered. Based on the reflectivity information from the manufacturer's data sheet, the absorber can be modeled as plane-boundary lossy dielectric with infinite thickness having an effective dielectric constant $\varepsilon_{eff} = 1.006$ and effective conductivity $\sigma_{eff} = 0.003 \text{ S/m}$ [15]. An asymmetrical-shaped anechoic chamber has been designed and constructed. The unique chamber geometry as shown in Figure 5 ensures that an electromagnetic ray will only reach the receiver antenna after a few reflections (except for those reflected from the conductive floor). The modeling of the asymmetric anechoic chamber is done for transmitter antenna height of 1 m. The wave propagation simulation also includes the effects of diffracted waves from the wedge-shaped walls and ceiling. Figure 6 shows that the simulation results converge after 5 bounces of the wave off the chamber structure.

The site attenuation deviations (SAD) with respect to theoretical NSA for 1-m transmitter height are shown in Figure 7. The predicted NSA is not expected to be close to ideal value because the 24-inch thick pyramid absorber has a poor reflectivity below 1000 MHz. The objective of the modeling is to ensure the predicted NSA is within $\pm 4 \text{ dB}$ tolerance prior to the chamber construction.

The results of NSA measurements for the asymmetric semi-anechoic chamber are shown in Figure 8. Generally, the NSA

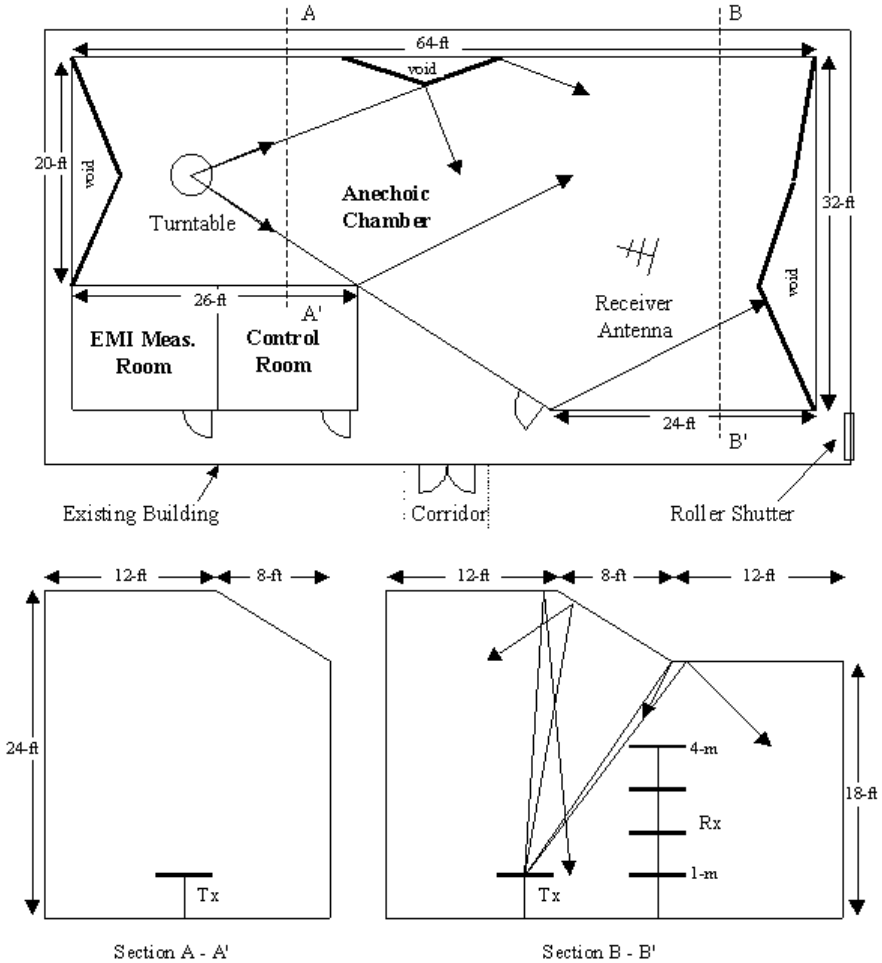


Figure 5. Floor plan and cross-sectional views of the asymmetrical-shaped chamber.

performances are within the ± 4 dB tolerance for frequencies from 80 MHz to 1000 MHz. At frequencies below 80 MHz, the large SAD may be attributed to a number of factors. Due to poor absorber reflectivity, the wave reflected from the ceiling, bounce off the conductive ground plane, and then propagates toward the receiver antenna may have a considerably large amplitude. Reflections from other chamber structures will also contribute to the deviation. If the asymmetric chamber has a height of 26 ft (instead of 24 ft), the modeling shows

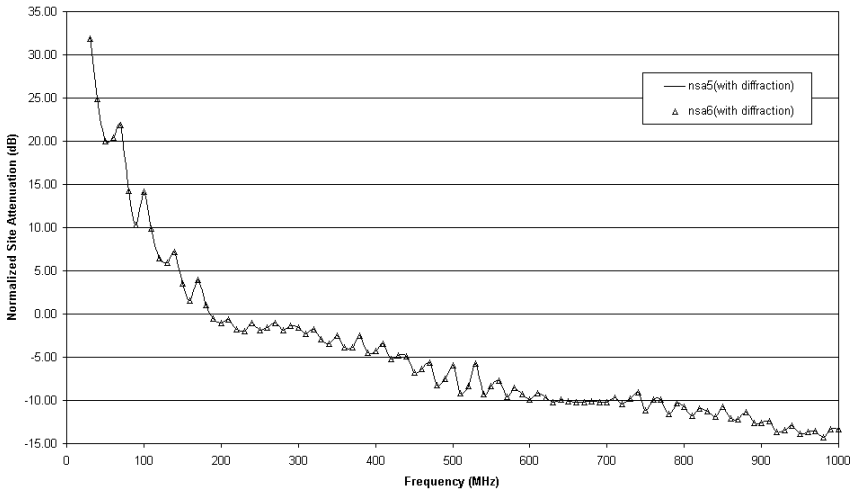


Figure 6. Predicted normalized site attenuation of the asymmetric anechoic chamber (horizontal polarization, $d = 10$ m, $h_e = 1$ m) for 5 and 6 bounces.

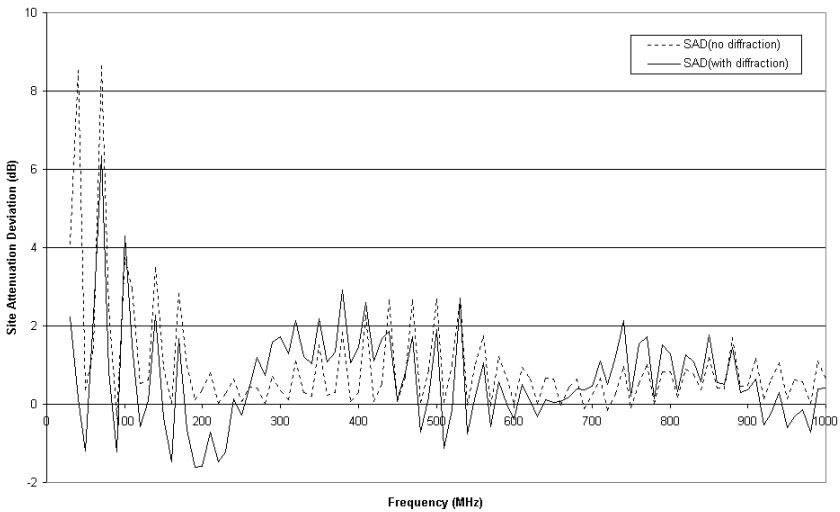


Figure 7. Predicted site attenuation deviations (SAD) of the asymmetric anechoic chamber (horizontal polarization, $d = 10$ m, $h_e = 1$ m).

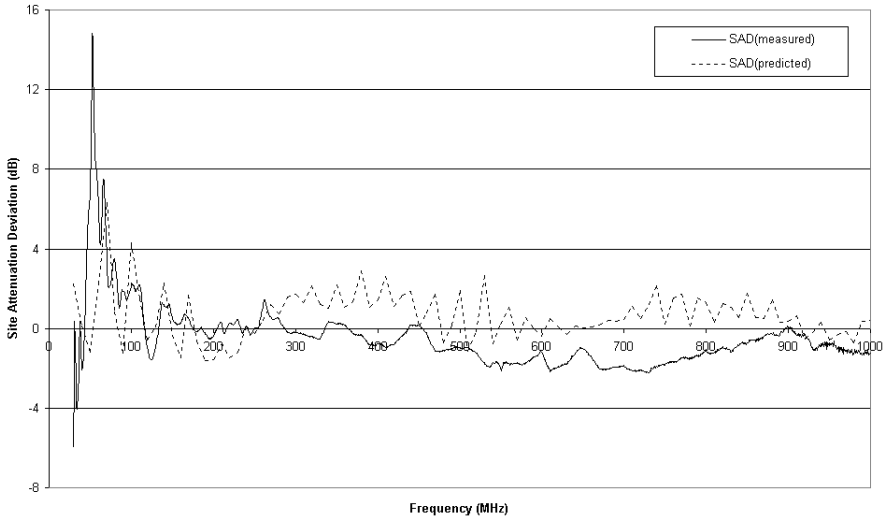


Figure 8. Comparison between measured and predicted SAD of the asymmetric anechoic chamber (horizontal polarization, $d = 10$ m, $h_e = 1$ m).

that a better result can be achieved.

Accurate antenna factors must be used in determining the measured NSA. Due to coupling to the ground plane and chamber walls, the antenna factors supplied by the manufacturer may be inadequate. Furthermore, the antennas are individually calibrated for horizontal polarization only. The operation of the antenna in non-uniform field also contributes to antenna factor errors.

The accuracy of the NSA measurements may be affected by impedance mismatch error, antenna separation distance error, frequency error, antenna factor frequency interpolation, antenna misalignment, and instrumentation error. In addition, the theoretical NSA model does not take into account the near-field effect where the $1/r^2$ and $1/r^3$ terms of electromagnetic field may be significant at frequencies below 80 MHz. This effect gives rise to excessive SAD at the low-frequency range.

4. CONCLUSION

The beam-tracing technique is a very useful tool for modeling of anechoic chamber. The path loss information at multiple receiver locations can be determined simultaneously as opposed to running a ray tracing simulation for each receiver location one at a time. Hence, the computing time is greatly reduced compared to ray-tracing technique. This feature is particularly useful in calculating the field strength at different heights of the receiving antenna in EMC site calibration procedure. If the room geometry is designed such that an electromagnetic ray from the transmitter will only reach the receiver antenna after a few reflections, the wave energy may be sufficiently damped after a few bounces off the absorbing walls and ceiling. Hence, lower cost RF absorbers can be used to make the anechoic chamber design more economical. The semi-anechoic chamber can be converted to a full anechoic chamber by placing removable pyramid absorber over the conductive floor.

ACKNOWLEDGMENT

This study is partially funded by the Malaysian Centre for Remote Sensing of the Ministry of Science, Technology and the Environment, Malaysia.

REFERENCES

1. Garn, H., E. Zink, and R. Kremser, "Problems with radiated emission testing at 3m distance according to CISPR 11 and CISPR 22," *Proceedings of the 1993 IEEE EMC Symposium*, 216–221, 1993.
2. Hansen D., D. Ristau, and P. Lilienkamp, "Correcting OATS antenna factors for small fully anechoic chambers," *IEEE International Symposium on EMC*, 219–223, 2000.
3. Holloway, C. L., R. R. DeLyser, R. F. German, P. McKenna, and M. Kanda, "Comparison of electromagnetic absorber used in anechoic and semi-anechoic chambers for emission and immunity testing of digital devices," *IEEE Transactions on EMC*, Vol. 39, No. 1, 33–47, February 1997.
4. Yang, C. F., B. C. Wu, and C. J. Ko, "A ray-tracing method for modelling indoor wave propagation and penetration," *IEEE Transactions on Antennas and Propagation*, Vol. 46, No. 6, 907–919, 1998.

5. Kimpe, M., H. Leib, O. Maquelin, and T. H. Szymanski, "Fast computational techniques for indoor radio channel estimation," *Computing in Science & Engineering*, Vol. 1, No. 1, 31–41, 1999.
6. Chen, S. H. and S. K. Jeng, "An SBR/Image approach for radio wave propagation in indoor environments with metallic furniture," *IEEE Transactions on Antennas and Propagation*, Vol. 45, No. 1, 98–106, 1997.
7. Fortune, S., "Efficient algorithms for prediction of indoor radio propagation," *48th IEEE Vehicular Technology Conference*, Vol. 1, 572–576, 1998.
8. Teh, C. H. and H. T. Chuah, "An improved image-based propagation model for indoor and outdoor communication channels," *Journal of Electromagnetic Waves and Applications*, Vol. 17, No. 1, 31–50, 2003.
9. Foley, J. D., A. V. Dam, S. K. Feiner, and J. F. Hughes, *Computer Graphics: Principles and Practice*, 2nd ed., Addison-Wesley, New York, 1996.
10. Murta, A., "A generic polygon clipping algorithm," Available online at <http://www.cs.man.ac.uk/aig/staff/alan/software/index.html>, April 1999.
11. Holloway, C. L. and E. F. Kuester, "Modeling semi-anechoic electromagnetic measurement chambers," *IEEE Transactions on EMC*, Vol. 38, No. 1, 79–84, February 1996.
12. Fante, R. L. and M. T. McCormack, "Reflection properties of the salisbury screen," *IEEE Transactions on Antennas & Propagation*, Vol. 36, No. 10, 1443–1454, 1988.
13. Kuester, E. F. and C. L. Holloway, "Improved low-frequency performance of pyramidal-cone absorbers for application in semi-anechoic chambers," *1989 IEEE International Symposium on EMC*, 394–398, 1989.
14. Janaswamy, R., "Oblique scattering from lossy periodic surfaces with application to anechoic chamber absorbers," *IEEE Transactions on Antennas & Propagation*, Vol. 40, 162–169, 1992.
15. Chung, B. K. and H. T. Chuah, "Modeling of RF absorber for application in the design of anechoic chamber," *Progress in Electromagnetics Research*, PIER 43, 273–285, 2003.

B. K. Chung graduated with a B.Eng. (Hons) in Electrical Engineering from the University of Malaya in 1992. He worked in the Design Department of Sony Electronics in Penang, Malaysia from 1992 to 1995. He then returned to the University of Malaya to undertake a research project and obtained his M.Eng. Sc. degree in Electrical Engineering in 1997. Since then he has joined the Faculty of Engineering, Multimedia University, as a lecturer. His research interests are in microwave systems, antenna design, remote sensing, electromagnetic compatibility, and electronic instrumentation and measurements.

C. H. Teh obtained his B.Eng. and M.Eng.Sc. in electrical engineering from University of Malaya and Multimedia University, respectively. From 1997 to 2001, he worked as a tutor at the Faculty of Engineering, Multimedia University. He is currently a lecturer at the same institution. His research interests include wave propagation and wireless communications.

H. T. Chuah obtained his B.Eng.; M.Eng.Sc., and Ph.D., all in electrical engineering, from the University of Malaya. He is currently the Dean of Faculty of Engineering, Multimedia University. Chuah was the recipient of the inaugural Young Engineer Award by the Institution of Engineers, Malaysia in 1991, the 1995 National Young Scientist Award (Industrial Sector) by the Malaysian Ministry of Science, Technology and the Environment, and the recipient of 1999 Malaysia Toray Science and Technology Award. His research interest are in applied electromagnetic, microwave remote sensing, and device physics.